Retraction

Retracted: Optimization and Mechanical Properties of TiO$_2$ Reinforced AA 7150 Composites Using Response Surface Methodology

Advances in Materials Science and Engineering

This article has been retracted by Hindawi, as publisher, following an investigation undertaken by the publisher [1]. This investigation has uncovered evidence of systematic manipulation of the publication and peer-review process. We cannot, therefore, vouch for the reliability or integrity of this article.

Please note that this notice is intended solely to alert readers that the peer-review process of this article has been compromised.

Wiley and Hindawi regret that the usual quality checks did not identify these issues before publication and have since put additional measures in place to safeguard research integrity.

We wish to credit our Research Integrity and Research Publishing teams and anonymous and named external researchers and research integrity experts for contributing to this investigation.

The corresponding author, as the representative of all authors, has been given the opportunity to register their agreement or disagreement to this retraction. We have kept a record of any response received.

References

[1] S. V. G. V. A. Prasad, V. Kamalakar, J. Madhusudhanan et al., "Optimization and Mechanical Properties of TiO$_2$ Reinforced AA 7150 Composites Using Response Surface Methodology," *Advances in Materials Science and Engineering*, vol. 2022, Article ID 5779840, 12 pages, 2022.

Research Article

Optimization and Mechanical Properties of TiO$_2$ Reinforced AA 7150 Composites Using Response Surface Methodology

S V G V A Prasad,[1] V. Kamalakar,[2] J. Madhusudhanan,[3] Puthalapattu Reddy Prasad,[4] G. Adilakshmi,[5] Nellore Manoj Kumar,[6] Anitha Gopalan,[7] Vinod Singh rajput,[8] and Nagaraj Ashok [9]

[1]*Department of Physics, Pithapur Rajah's Government Autonomous College, Kakinada 533001, Andhra Pradesh, India*
[2]*Department of Physics, Vel Tech Rangarajan Dr. Sagunthala R&D Institute of Science and Technology, Avadi, Chennai, Tamil Nadu, India*
[3]*Department of Biotechnology, Anand Institute of Higher Technology, Chennai 603103, TamilNadu, India*
[4]*Department of Chemistry, Institute of Aeronautical Engineering, Dundigal, Hyderabad 500043, Telangana, India*
[5]*Scienuvo R & D Services, Hyderabad 500038, Telangana, India*
[6]*Department of Physics, SCSVMV Deemed University, Enathur, Kanchipuram 631561, Tamil Nadu, India*
[7]*Department of Electronics and Communication Engineering, Saveetha School of Engineering, SIMATS, Chennai 602105, Tamilnadu, India*
[8]*Department of Mechanical Engineering, Nowgong Engineering College, Chhatarpur, Nowgong, Madhya Pradesh, India*
[9]*Faculty of Mechanical Engineering, Jimma Institute of Technology, Jimma University, Jimma, Ethiopia*

Correspondence should be addressed to Nagaraj Ashok; nagaraj.ashok@ju.edu.et

The goal of this research is to increase the performance of AA 7150 reinforced with TiO$_2$ microparticles by optimizing the stir casting parameters. The response surface method's central composite design technique was used to optimize the three stir casting factors of stirring temperature (A), stirring speed (B), and stirring time (C). The ultimate tensile strength, hardness, impact strength, elastic modulus, and compressive strength were all tested. With the aid of analysis of variance, it was discovered that it had a substantial influence on the test samples' characteristics responses. 5 quadratic experiments were linked using factors' characteristics. At a level of 95% confidence, the models were found to be statistically important, and the variations were found to be less than 5%. The response surface was used to assess the parameter interaction profile. Each interaction's contour plots provided a range of stirring settings within which each property may be maximized.

1. Introduction

A typical practice in engineering is to strengthen an alloy matrix with ceramic particles [1]. The resulting materials are useful in an extensive range of fields. Numerous analyses have focused on the creation of high-performance composites due to the adaptability of alloy in modern engineering fields [2, 3]. The alloy and its composite have a higher strength-to-weight ratio than steel, making them better suited for lightweight and fuel-efficient applications in automobiles and airplanes. The 7000 family of aluminum alloys includes Al 7150-T6, which has excellent mechanical qualities and may be employed in a extensive range of fields [4, 5]. Ceramic nano and microparticles, based ceramic particles, have been the focus of recent research aimed at enhancing alloy characteristics. As reinforcing particles in metal matrices, titanium-based particulates have a wide range of uses [6, 7]. For the Al 7150 matrix reinforced with SiC and TiC, stir casting was used to add 5% silicon carbide and 5% titanium carbide. With the incorporation of 5% silicon carbide and 5% titanium carbide, it was found that the YS, UTS, and IS were all the maximum [8]. With the help

of TiC, [9] reinforced Al 7150 at various percentages of 3, 4, 5, 6, or 7%. A seven weight percentage increase in particle concentration increased microhardness, YS, and UTS. The hardness and bending strength of Al 7150 were improved when 1.5, 3, 4.5, and 6 wt% of TiB2 were injected into the alloy as observed by [10]. According to their research, the microstructure demonstrated a particle dispersion inside the matrix, increasing its characteristics. At particle dosages of 4, 8, and 12 wt%, titanium boride dispersion in Al 7150 matrix improved tensile strength and hardness, according to the research of [11, 12]. Even at 9 wt% TiC inclusion, the yield and tensile strength of Al 7150 were improved by TiC infusion. Adding titanium carbide at 3–7% of the aluminum alloy resulted in the same pattern. It was found that the microhardness, YS, and UTS of the stir cast product as particles increased [13–15].

At a concentration of 7%, the greatest increase in strength was observed. For Al 7150, titanium dioxide was used to boost compressive and tensile strength, with the maximum increase occurring at a titanium dioxide concentration of 15% weight. Reference [16] reinforced Al 6061 with titanium dioxide with an average particle size of 50 m. When the particle content was increased from 1 to 3 wt%, the hardness and ultimate tensile strength improved by 20.7, 52.6, and 66.7 and 31.6, 55.8, and 89.5%, respectively. The titanium dioxide particle-reinforced composite had better characteristics than the basic metal, corresponding to the analyses. Researchers [17, 18] developed TiO_2–AA 7150 composites with varied titanium dioxide particle concentrations of 5, 10, and 15% using the stir casting method. A 10% increase in the percentage of particles increased the mechanical parameters, tensile strength, flexural and compressive strengths, and hardness, The visualization technique has been used by [19, 20] to examine the impact of the stir casting factors on the supply of reinforcing materials. There is a significant improvement in mechanical qualities when the impeller is placed 40% away from the standard 45° blade angle. CFD models were used to examine the impact of vortex pressure, generated through stirring, on the MMC process [21].

Using Taguchi's experimental design, the researchers found that increasing the vortex height improved mechanical properties. Microstructural analysis [22] was also carried out in the study of the impact of stir casting factors on composite structural characteristics. According to the microstructural analysis, the reinforcing particles are uniformly dispersed, which leads to an increase in mechanical characteristics for the composites over time. The ideal stir casting factors for processing MMC have never been determined through RSM optimization, despite the fact that a variety of approaches have been used [23]. Previously studied influences on Al 7150's properties from variables such as stirring temperature, duration, and speed were not considered. Additionally, impeller rotation direction, blade angle, stirrer height, and reinforcement feed rate are all process variables [24, 25]. It is vital to figure out how these variables affect the microstructure so that you can optimize for alloy improvement under the best circumstances. A study conducted by [26, 27] shows that the UTS,

microhardness, IS, EM, and CS for Al 7150/10% weight microparticles of TiO2 (mean size 13 mic) was best achieved at 10%, according to [28, 29] which found that 10% yielded the best performance for the microparticles. The purpose of this work is to investigate the mechanical properties of composites synthesized using a variety of parameters utilizing RSM.

2. Materials and Methods

2.1. Composite Preparation. This experiment made use of an aluminum alloy ingot, AA 7150-T6. Table 1 shows the spectrometer results for the chemical composition, whereas Table 2 lists the physical attributes. Crucible made of graphite was used for the stir casting procedure. The melt was warmed to 500°C for 10 minutes before TiO2 microparticles of 13 microns were injected at a concentration of 10 weight%. The specimens were created in accordance with the central composite design plan based on the trial runs listed in Table 3 and Table 4. As reported by [15], the wettability of the matrix was increased by adding magnesium to the melt.

2.2. Testing Procedure. UTM equipment was employed to calculate the tensile strength (TS) of machined specimens 30 mm long and 5 mm in diameter (Instron 3369 Series). With a crosshead speed of 3.0 mm/min, ASTM *E* 8/E8M-2-compliant loads of 10,000 N were applied at a rate of 10^{-4} per second. The specimens were subjected to a 100 kN load at a cross-speed of 1 mm/min using universal testing equipment in accordance with ASTM E09-9. Each specimen was subjected to a Vickers microhardness test in accordance with ASTM *E* 384–17 utilizing a load of 10 N for ten seconds on its surface. Also, the high strain impact toughness of a specimen $10 \times 10 \, mm^2$ was studied by monitoring the absorbed energy until failure with a 300 N pendulum (ASTM E-23).

2.3. Experiment Design. The experimental procedure begins with the design of experiments utilizing the response surface methodology, which optimizes processing factors. Response surface methodology examines the relations among processing and responding factors. It is a routine trend to utilize the response surface methodology to model and analyze processes in which the rate is determined by multiple variables. A central composite design containing a level-three component was implemented using the Minitab 19 program. For each attribute evaluated, twenty experimental runs were undertaken, including six axial runs, eight factorial runs, and six repeats at the center point. The relationship between process factors and predicted responses was established using (1). The predicted response is denoted by *Z*, the intercept is denoted by A, the linear coefficient is denoted by B for first-order expressions, the quadratic coefficient is denoted by C for second-order expressions, the interaction coefficient is denoted by *D*, and the random error is denoted by E. The equation expresses the model of the first-order polynomial.

$$Z = A + BX_1 + CX_2 + C_nX_n + E. \tag{1}$$

Table 1: Composition of the alloy Al 7150 employed in the investigation.

Component	Zinc	Magnesium	Copper	Silicon	Iron	Titanium	Copper	Aluminium
Quantity (%)	8.2	2.9	0.15	0.2	0.2	0.1	0.22	Remaining

Table 2: Properties of aluminium 7150.

Properties	Ultimate tensile strength	Poisson ratio	Relative density
Aluminium 7150	607	0.33	2.84

Table 3: Factor levels in the experiment's design.

Factors	Levels		
	Low	Medium	High
(A)	550	650	750
(B)	450	550	650
(C)	10	15	20

Table 4: Experimental results, levels, and outputs.

Experimental run	Levels			Factors			Responses				
	A(°C)	B(rpm)	C(min)	A(°C)	B(rpm)	C(min)	YS	UTS	EM	El	IM
1	−1	−1	−1	550	450	10	501	581	82.6	8.76	4.21
2	0	0	−1.68	550	450	10	525	642	90.1	7.84	5.31
3	0	0	0	550	450	10	529	689	91.4	7.51	5.74
4	0	0	0	550	550	15	546	635	86.5	7.52	5.46
5	0	0	0	550	550	15	575	719	95.3	6.79	6.41
6	0	1.68	0	550	550	15	588	682	98.2	6.43	6.86
7	1	1	−1	550	650	20	522	600	79.4	7.82	4.86
8	−1	1	1	550	650	20	559	622	88.6	7.99	5.51
9	−1.68	0	0	550	650	20	574	637	92.1	6.62	5.90
10	1.68	0	0	650	450	15	530	634	87.3	8.55	5.17
11	0	0	0	650	450	15	558	715	92.3	7.24	5.86
12	1	−1	1	650	450	15	564	734	98.5	7.12	6.13
13	0	−1.68	0	650	550	20	579	672	92.6	8.08	5.78
14	−1	−1	1	650	550	20	601	745	96.5	7.34	6.84
15	0	0	0	650	550	20	629	771	102.3	6.09	7.15
16	1	1	1	650	650	10	561	628	86.7	8.47	5.00
17	0	0	1.68	650	650	10	582	665	91.2	7.12	5.66
18	−1	1	−1	650	650	10	618	692	93.2	6.83	6.16
19	1	−1	−1	750	450	20	524	600	84.5	8.17	4.24
20	0	0	0	750	450	20	531	657	86.8	6.94	4.87

Mean Square Error and RMS Deviation were used to assess the models' accuracy. These are anticipated benchmarks for the coefficient of correlation for forecast and adjusted data. It is recommended by [30] that the temperature range be in the range of 550 to 750°C, the duration be somewhere between 10 and 20 minutes, and the rotational speed be somewhere between 450 and 650 rpm.

3. Results and Discussion

3.1. ANOVA and Regression Models. Using Table 5, we can see that the P values for processing parameters are all lesser than 0.05, showing that these factors are significant because they affect the reaction size. The $A * A$ and $C * C$ squared interactions are technically important; however, the $B * B$ interaction is not. Similarly, A, B, and C parameters

TABLE 5: Analysis of variance for ultimate tensile Stress.

Source	Df	Seq SS	Contribution (%)	Adj SS	Adj MS	F value	P value
A	1	8276.2	37.12	8359.8	8359.4	229.45	0.000
B	1	2972.4	8.12	2972.1	2972.12	123.64	0.000
C	1	7908.5	28.24	7909.7	7909.5	234.51	0.000
A * A	1	4169.3	13.91	4175.7	4175.4	129.63	0.000
B * B	1	609.4	2.32	608.4	608.5	17.08	0.121
C * C	1	1828.6	5.98	1828.6	1828.5	134.24	0.000
A * B	1	459.4	1.71	472.3	472.5	13.12	0.056
A * C	1	8.9	0.04	10.2	10.3	0.27	0.627
B * C	1	69.8	0.25	69.4	69.7	1.89	0.178
Error	16	615.4	2.31	616.5	37.32		
Total	25	26917.9	100				

contribute 37.12, 8.12, and 28.24%, respectively, demonstrating that the components are relevant in decreasing order of A, B, and C. The input variable is taken into account by the 2nd order polynomial function for UTS.

Ultimate Tensile Strength $= 229 + 6.15A + 0.4908B + 0.4657C\,0.1941A * A\,0.000405B * B\,0.002861C * C + 0.002286A * B$

$$+ 0.00086A * C\,0.00081B * C. \tag{2}$$

P values are less than 0.05 in Table 6, which indicates that the linear terms of Sintering temperature, speed, and time are important, accounting for 41.24%, 21.27%, and 30.15% of the total, respectively. As the input parameter changes, the hardness response of the features changes accordingly. It does not matter what the square terms A * A, B * B, C * C, or A * B, A * C, or B * C mean. According to the linear terms, the temperature of the stirring is the most important, followed by the time of the stirring. Stirring speed had the least impact on any of the three variables. A 2nd order polynomial function for Hd is presented in

Hardness $= 186.7 + 50.5A + 0.4630B + 5.29C\,0.81A * A\,0.000189B * B\,0.0444C * C + 0.0260A * B$

$$+ 0.557A * C\,0.00197B * C. \tag{3}$$

Hardness is denoted by Hd, stirring temperature is denoted by A, stirring speed is denoted by B, and stirring time is denoted by C. ANOVA examination of the impact strength revealed a significant relationship between the response and the input factors. The squared relations A * A and C * C are not as substantial as the linear factors A, B, and C. Responses to A * B, A * C, and C * C are unaffected. A, B, and C each contribute 30.15%, 15.01%, and 27.14%;

therefore, A is the most important factor to consider and then comes the time of stirring, with the speed of stirring having the least impact. Table 7 shows ANOVA on IM.

At the 95% confidence and 5% significance levels, the elastic modulus's reaction to process variables is summarized in Table 8. It is clear from the plots that there is a significant correlation between the processing parameters A, B, and C in the linear model with P value.

Impact Strength $= 13.15 + 36.1A + 0.379B + 3.84C\,0.5A * A\,0.000156B * B\,0.0313C * C + 0.0165A * B\ (5)$

$$+ 0.368A * C\,0.00102B * C. \tag{4}$$

A * A and C * C squared interactions had no effect on the answer; however, B * B has an effect. Statistically, the interfaces A * B and B * C are not significant, whereas A * C is. There is a 36.89% contribution from parameter A (stirring temperature), followed by 18.12% from parameter B (stirring time) and 26.04% from parameter C (stirring speed). The input variable was incorporated into a second-order polynomial model.

Table 6: Analysis of variance on hardness.

Source	Df	Seq SS	Contribution (%)	Adj SS	Adj MS	F value	P value
A	1	8607.4	41.24	8601.8	8602.4	301.41	0.000
B	1	4668.1	21.27	4681.2	4682.1	235.14	0.000
C	1	6559.4	30.15	6571.3	6571.4	261.5	0.000
A * A	1	231.4	1.27	231.4	231.5	10.01	0.069
B * B	1	3.7	0.01	3.8	3.81	0.12	0.752
C * C	1	80.02	0.39	80.1	80.2	3.05	0.590
A * B	1	170.1	0.89	170.2	170.1	6.81	0.091
A * C	1	192.4	0.87	195.4	194.8	7.81	0.071
B * C	1	97.4	0.46	97.4	97.3	3.89	0.357
Error	53	369.1	3.45	26.4	26.5		
Total	62	20978.02	100				

Table 7: ANOVA on impact strength.

Source	Df	Seq SS	Contribution (%)	Adj SS	Adj MS	F value	P value
A	1	7971.2	30.15	7971.4	7971.6	218.7	0.000
B	1	4354.1	15.01	4835.3	4829.1	134.34	0.000
C	1	7274	27.14	8364.8	8364.8	235.54	0.000
A * A	1	4901.7	18.04	4904.4	4897.6	134.84	0.000
B * B	1	459.8	2.01	467.4	467.54	13.04	0.049
C * C	1	1169.3	5.34	1169.3	1169.4	33.16	0.000
A * B	1	69.7	0.27	69.4	69.5	0.27	0.594
A * C	1	608.4	2.35	609.4	609.54	6.48	0.079
B * C	1	10.1	0.04	10.2	10.26	17.94	0.864
Error	16	612.4	2.19	617.4	37.14	2.13	0.192
Total	25						

Table 8: Analysis of variance for elastic moduli.

Source	Df	Seq SS	Contribution (%)	Adj SS	Adj MS	F value	P value
A	1	7001.4	36.89	7001.5	7001.52	276.61	0.000
B	1	5254.5	18.12	5254.6	5254.62	204.14	0.000
C	1	5998.6	26.04	5998.61	5998.62	238.51	0.000
A * A	1	1.1	0.02	1.1	1.1	0.05	0.851
B * B	1	249.5	9.24	249.6	249.6	6.27	0.042
C * C	1	40.2	0.31	40.1	40.1	1.62	0.0227
A * B	1	69.4	0.39	69.4	69.3	2.79	0.112
A * C	1	186.2	5.84	186.3	186.4	4.39	0.026
B * C	1	27.2	0.22	27.3	27.2	2.05	0.321
Error	53	137.6	2.93	137.6	26.12		
Total	62	18965.6	100				

$$\textbf{Elastic Modulus} = 42.2 + 82.3A + 1.033B + 5.86C22.29A * A0.00571B * B0.0815C * C + 0.0184A * B$$
$$+ 0.643A * C0.00223B * C. \tag{5}$$

Elastic modulus (EM). A, B, and C have P values < 0.05, which indicates that they are substantial and contribute 38.14%, 7.24%, and 30.12% correspondingly to the composite's compressive strength response, as indicated in Table 9. Correlations A * B, A * C, and B * C are irrelevant but the square terms A * A, B * B, and C * C are substantial. According to linear terms, the temperature of the stirring is the most important, followed by the time of the stirring.

TABLE 9: ANOVA on compressive strength.

Source	Df	Seq SS	Contribution (%)	Adj SS	Adj MS	F value	P value
A	1	70026	38.14	70026	70124	369.14	0.000
B	1	13541	7.24	13541	13542	70.08	0.000
C	1	59964	30.12	59964	59964.2	293.14	0.000
$A*A$	1	19245	9.97	19245	19245.4	99.41	0.000
$B*B$	1	1517	6.84	1517	1517.7	7.31	0.000
$C*C$	1	7669	5.14	7669	7669.2	40.12	0.009
$A*B$	1	749	0.39	749	749.8	4.01	0.091
$A*C$	1	1162	0.3	1162	1162.4	6.02	0.082
$B*C$	1	3174	1.29	3174	3174.4	15.81	0.063
Error	54	1049	0.57	10512	189.6		
Total	63	178096	100				

Stirring speed had the least impact on any of the three variables. The equation represents compressive strength (Pa).

$$\textbf{Compressive Strength} = 80.9 + 133.8A3.018B + 24.38C18.81A*A0.00173B*B0.4381C*C + 0.055A*B + 1.361A*C0.0111B*C. \tag{6}$$

3.2. Coefficient of Correlation for Mechanical Characteristics.
Table 10 lists the correlation coefficients, R^2 (adj), R^2 (pred), and R^2 (the variance among R^2 (adj) and R^2 (pred)). If $R^2 = 98.41\%$ for UTS, then there is a strong correlation between the model and the dependent variable, with the model accounting for 98.41% of the observed variation. $R^2 =$ Adj R^2 (adjustment) has a value of 97.61%, while Pred R^2 has a value of 94.42%. A credible model should have at least a 20% difference between the two regression coefficients because the difference between the two coefficients is at least 20% in the UTS. R^2 values of 95.04% for hardness, 96.29% for impact and elastic modulus, and 97.03% for compressive strength indicate that the model accurately characterizes the relationships by more than 90% of the variance. Elastic modulus, compressive strength, and hardness all have R^2 (%) values under 20%, indicating they meet the criteria for good correlation. There are so few variations from a straight line; it is safe to say that this model holds true for the vast majority of data. As can be seen in Figures 1(a)–1(e), where the dots are clustered along a line, the scatter plot of the residual data versus the fitted data shows that the data are heteroskedastic. A good model is one where the response residuals are evenly spread around the mean value.

3.3. Analysis of the Response Surface and Contour Plot.
The greatest tensile strength can be achieved by plotting the response surface and contours. Temperature (Tm) and speed (Sp) of stirring have an impact on a composite's UTS. Two process parameters are plotted as a function of the other variable, and the model is shown as a graphical representation of this relationship. X and Y axes are used to plot input variables, and the Z axis is used for the response. Figure 2(a) depicts the response surface for a continuous 15-minute period for the speed-temperature interaction. In contrast, at 550 rpm and 750°C, the maximum tensile strength response value dropped significantly. As a result, the final tensile strength is strongly influenced by the relationship between speed and temperature. Shifting a parabolic reflection profile with inflection points at 750°C and 550 revolutions per minute resulted in an inflection point pressure of 664 MPa. Using a 15-minute timer, Figure 2(b) shows how interaction temperature affects UTS. Temperature and pace have a significant impact on tensile strength. Part A's ideal strength range is between 600 and 640 MPa when temperature and speed are taken into account, which is between 721 and 841°C and 440–635 rpm.

The UTS of composites is affected by the relationship between stirring time (T) and speed (Sp). At a constant 650°C Tm, the relationship between stirring duration and speed can be shown in Figure 2(c). As the T and Sp grew beyond 500 rpm, a significant negative speed-temperature interaction occurred, consequential in a reduction in overall strength. As a result of the right speed and length of stirring, particles are more evenly dispersed in the melt. Speeds greater than 500 rpm resulted in turbulent churning that trapped gas and created blow holes, resulting in decreased tensile strength. There was a positive trend in the time and speed charts for both stirring speeds. Figure 2(d) displays the contour plot of the two variables, which are separated into portions by the boundary lines shown in the figure. As shown in Plot A, a churning speed of 462–555 rpm paired with an appropriate stirring period (between 20 and 22.5 minutes) can produce an ideal strength range of 660–675 MPa. This is the best part of the graph.

TABLE 10: Correlation coefficient.

Parameters	R^2 (%)	R^2 (Adj) (%)	R^2 (Pred) (%)	γR^2 (%)
UTS	98.41	97.61	94.42	<20
Hardness	95.04	94.81	92.86	<20
Impact strength	96.29	95.24	93.24	<20
Elastic modulus	97.03	96.41	94.86	<20
Compressive strength	98.42	97.42	95.16	<20
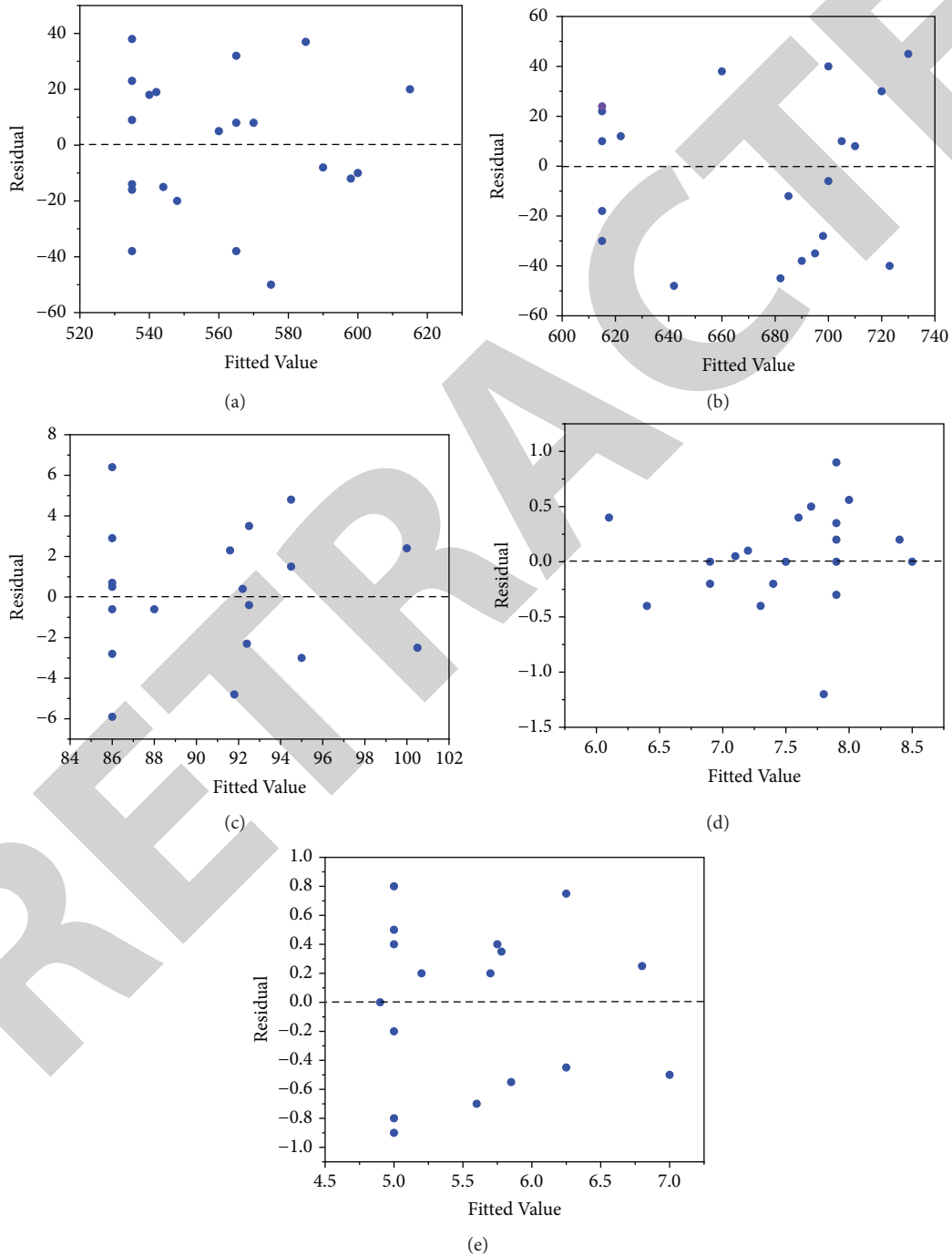
FIGURE 1: The residuals for responses are plotted using the normal probability distribution. (a) UTS, (b) H_d, (c) IS, (d) EM, and (e) CS.

(a)

(b)

(c)

(d)

(e)

(f)
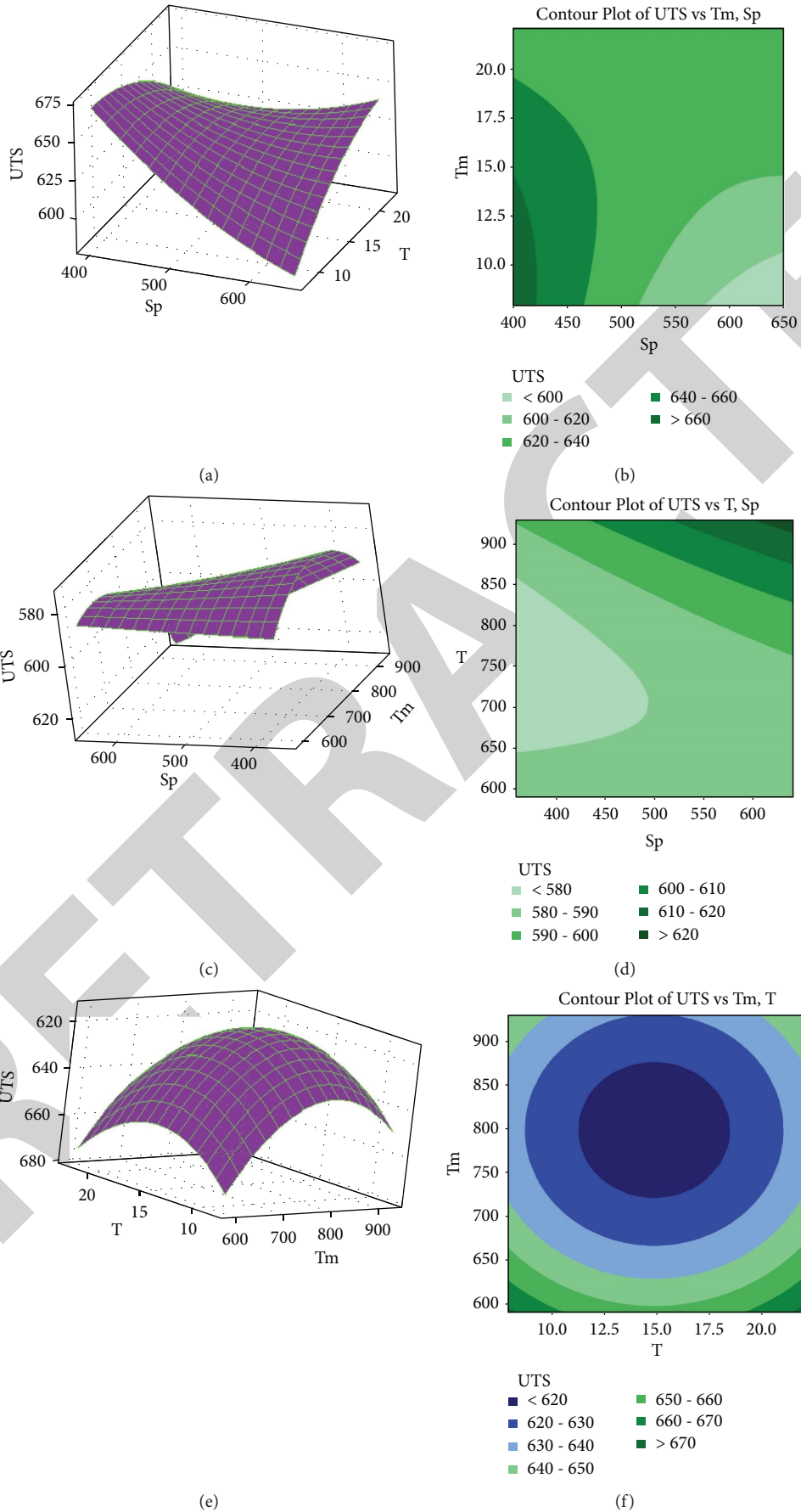
Figure 2: Reaction surface plots and contour plots for interactions show the effect of stirring constraint on the final TS of the generated mixtures. (a, b) Sp and Tm, (c, d) Sp and T, (e, f) Tm and T.

A composite's tensile strength is influenced by the temperature-stirring interaction (T) (Tm). When the temperature and time are properly controlled, the TS of the aluminum composite can be indicated in Figure 2(e). Increasing temperature and time both enhanced ultimate tensile strength; however, the temperature and time interaction cause a decrease in strength over 750°C. The temperature profile becomes parabolic at 750°C; however, the time profile shows a linear collaboration of positive gradients. The maximum strength of 665.8 MPa was achieved by combining the two parameters of 750°C and 22.5 minutes. Figure 2(f) depicts the relationship between ultimate tensile strength (T) and interaction time (T) and temperature (T). Boosting the amount of time and temperature had the desired effect of increasing strength. At 715–750°C and a length of 19.4–22.5 minutes, "A" determined the area of optimal strength that encompasses the value of 620–670 MPa.

Vickers microhardness of composite is affected by the interplay between stirring temperature (Tm) and speed (Sp). There was a gradual hardening of the material as the speed and temperature increased from −1 level. That the composite's hardness is influenced by the interaction between these two properties is evident from this. When speed and temperature were used as inputs, the concave profile shown in the picture was chosen. An interaction of 650 rpm and 835°C resulted in a maximum hardness of 119.2 HV. The picture also illustrates how the interaction affects the microhardness's response. Vickers microhardness of composites is affected by the interplay between stirring time (T) and stirring speed (Sp). The curve of Sp was concave, whereas the profile of stirring time was linear and positive, as depicted in the graph.

Stirring and temperature (Tm) time (T) affect the Vickers microhardness of a composite. Vickers microhardness of aluminum composite strengthened with TiO_2 ceramic microparticles at 500 rpm is shown to be impacted by the interplay of stirring duration and temperature. Hardness increased in lockstep with both temperature and elapsed time. This demonstrates that the composite's hardness is dependent on the interplay between these two variables. A concave temperature profile was shown whereas a linear one was shown for a time of 600 revolutions per minute at 835°C producing the maximum hardness of 119.2.

3.4. Impact Strength Response Surface and Contour Mapping.

The impact strength of the composite is affected by the interplay between stirring temperature (Tm) and speed (Sp). Impact strength increased with stirring speed, temperature, and speed; however, at 550 rpm stirring speed and 750°C temperature, impact strength decreased. As a result, the speed-temperature interaction pattern has a strong association with impact strength. With the ends facing down, the two experimental parameters shifted a parabolic profile.

Temperatures of 750°C and 550 rpm are the two sites of inflection, which provide a peak range of 5.27 J/m^2. At temperatures between 675°C and 842°C and speeds between 440 and 635 rpm, the interplay of temperature and speed yielded a maximum strength of more than 5.0 MPa in Portion "A.".

Speed and temperature had a substantial detrimental impact on strength when the rpm was greater than 500. With the proper speed and time of stirring, particles may be evenly dispersed in the melt. Turbulence, which causes gas entrapment and blowholes, reduces the strength of a mixture when it is stirred at more than 500 rpm. Stirrer speed increased linearly with a positive temporal gradient over time.

An impact composite's strength is influenced by the temperature-stirring time interaction (T) (Tm). Over 750°C, the temperature and time effect interacts in a negative way, resulting in an overall decrease in the impact strength. A 750°C inflection point marks the stirring temperature profile while stirring duration determines the positive gradient's linear interaction profile. When the two variables were merged, the energy output was 5.32 J/m^2 at 750°C and 22.5 minutes. The strength of the impact is affected by the contour plot of interaction duration against temperature. The impact strength was improved by increasing the time and temperature. At 725–785°C and 21.5–22.5 min, the portion labeled "A" found the spot for maximum strength, which is between 5.3 and 5.4 J/m^2. Figure 3 displays the reaction surface plot and contour plot for relations to show the impact strength of the generated composite as a result of stirring parameters. (a, b) Sp and Tm, (c, d) Sp and T, and (e, f) Tm and T.

Two elements were coupled to produce a parabolic interaction profile with inflection points at 750°C and 500 rpm, with the point of inflection reaching 95.5 GPa. Variations in temperature and speed interact with variable elastic moduli, and this graphic shows where those moduli are at different points in time. Thermal and mechanical interactions in Segment "A" result in a maximum strength range of about 94–96 MPa, which can be achieved by running the motor at temperatures between 780°C and 824°C and speeds between 475 and 580 rpm.

3.5. Mapping of Compressive Strength Using Response Surface and Contour Data.

The compressive strength of a composite is affected by the relationship between stirring temperature (Tm) and speed (Sp). Compressive strength increased over time as both speed and temperature increased. Because of this, the strong response is dependent on the interactions. The concave shape depicted in the image was the result of the two input factors speed and temperature. At 650 revolutions per minute and 820°C, the highest strength of 484.3 MPa was achieved.

The impact on composite compressive strength of the interplay between stirring time (T) and temperature (Tm) during stirring is as follows. For aluminum composites enhanced with TiO2 ceramic microparticles generated at a persistent velocity of 550 revolutions per minute, the connection between stirring duration and the temperature was clearly visible. Thus, the interplay between the two parameters is critical to the composite's strength. It was apparent that the temperature had a parabolic profile with both edges facing down, whereas time had a linear profile that

(a)
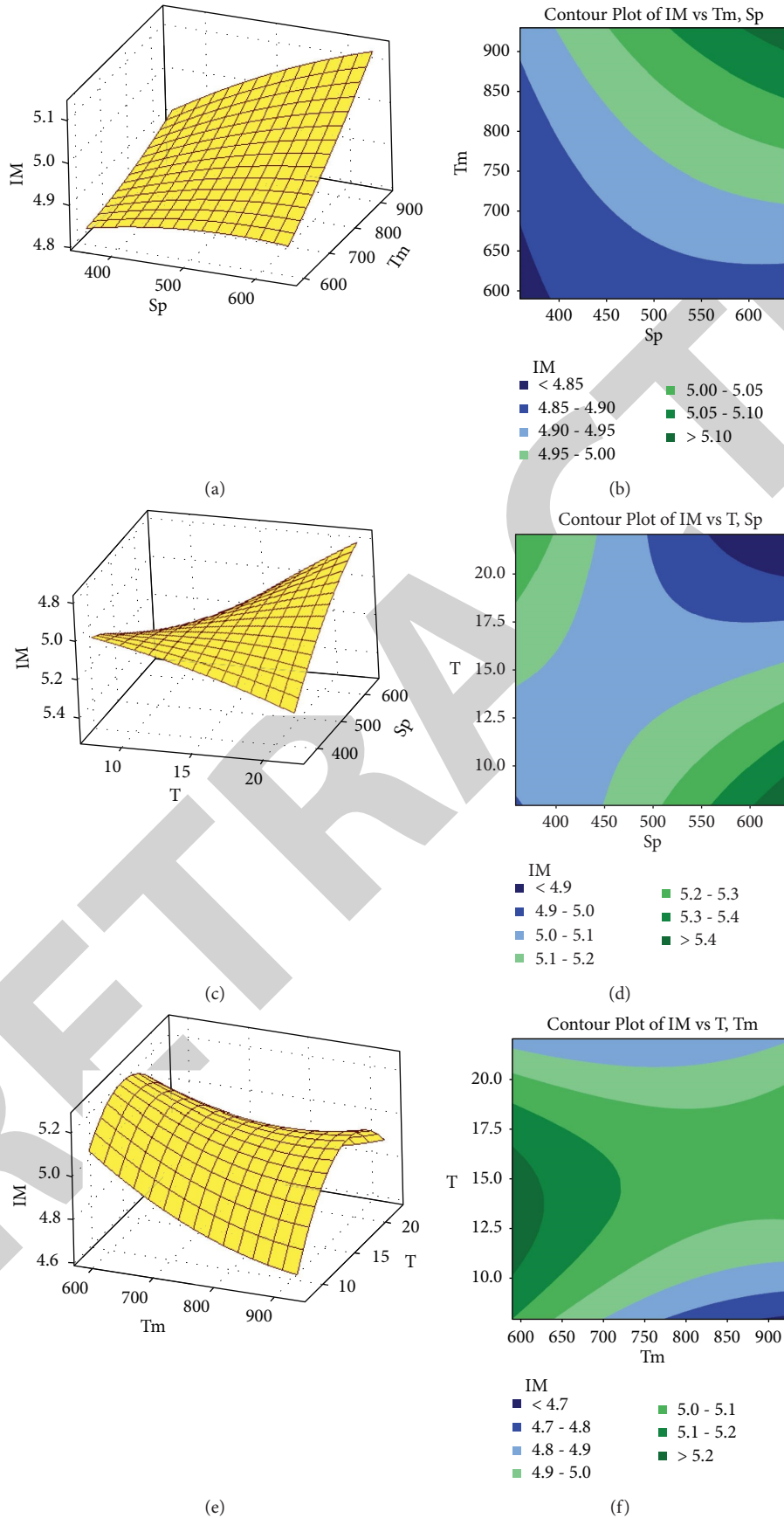

(b)

(c)

(d)

(e)

(f)

Figure 3: The reaction surface plot and contour plot for relations show the impact strength of the generated composite as a result of stirring parameters. (a, b) Sp and Tm, (c, d) Sp and T, and (e, f) Tm and T.

TABLE 11: The optimal parameters and outcomes. Overall, the desirability rating is 0.94.

	Optimal parameters		
	Temperature 780.1°C	Speed 568 rev/min	Time 23 minutes
	Predicted values	Experimental value	Deviation (%)
Compressive strength	496.8 Mpa	489.4 Mpa	1.51
Elastic modulus	98.2 GPa	101.5 GPa	2.82
Impact strength	5.4 kJ/m^2	5.67 kJ/m^2	4.38
Microhardness	120.4 HV	118.4 HV	1.98
Ultimate tensile strength	660.5 MPa	639.4 MPa	2.59

rose upward. At 650 rpm and 22.5 minutes, a maximum force of 486.8 MPa was achieved. Compressive strength is shown in the figure to be dependent on the collaboration.

3.6. Model Testing and Optimization. Minitab 19 was used to optimize the stirring temperature, speed, and time by means of the RSM. The tensile strength was increased by varying the independent variables from the lowest to the highest possible values. Optimization was performed at a 95% confidence level with no constraints, while the lesser and higher levels of all parameters were fixed. According to Table 11, optimum values for UTS, microhardness, IS, EM, and compressive strength (Table 11) were found. Stirring at 568 rpm, 780.1°C, and 23 minutes provides the optimum overall tensile strength. 568 rpm, 780.1°C, and 23 min were utilized to confirm the experimental run's speed, temperature, and time inputs. Table 11 shows the average results of the various experiments. Given that each property's variance is less than 5%, we can say with confidence that experimental results and anticipated results are good, proving that the model is accurate.

4. Conclusion

AA 7150/TiO2 composites were created using the stir casting process by altering the method's three processing parameters. The UTS, hardness, IS, EM, and CS all behave differently depending on the interplay between these properties. The analysis of variance revealed that the stirring constraints had an effect on each characteristic; however, the chosen square interactions had a significant effect at a 95% confidence level. Over 94 percent of the data was adequately represented by the five models constructed for the statistically significant attributes as determined by the correlation coefficient. Reaction surfaces revealed a high dependence of each variable on the relationships between the processing parameters. When the temperature was less than 650 °C and the speed was less than 550 rpm, there was a favorable effect on the responses. Additionally, a stirring time of up to 30 minutes may be necessary to provide a uniform dispersion, which aids the reaction.

Data Availability

The data used to support the findings of this study are included within the article.

Conflicts of Interest

The authors declare that there are no conflicts of interest regarding the publication of this article.

Acknowledgments

References

[1] J. A. Jeffrey, S. S. Kumar, V. A. Roseline, A. L. Mary, and D. Santhosh, "Contriving and assessment of magnesium alloy composites augmented with boron carbide VIA liquid metallurgy route," *Materials Science Forum*, vol. 1048, pp. 3–8, 2022.

[2] M. S. Kumar, S. R. Begum, C. I. Pruncu, and M. Shahedi Asl, "Role of homogeneous distribution of SiC reinforcement on the characteristics of stir casted Al-SiC composites," *Journal of Alloys and Compounds*, vol. 869, Article ID 159250, 2021.

[3] V. Mohanavel, M. Ravichandran, S. Suresh Kumar, M. Melwin Jagadeesh Sridhar, S. Dineshkumar, and M. M. Pavithra, "Microstructural and tribological characterization of Al/EGG shell ash composites prepared by liquid metallurgy process," *Journal of the Balkan Tribological Association*, vol. 26, no. 2, pp. 319–326, 2020.

[4] M. S. Kumar, C. I. Pruncu, P. Harikrishnan, S. R. Begum, and M. Vasumathi, "Experimental investigation of in-homogeneity in particle distribution during the processing of metal matrix composites," *Silicon*, vol. 14, pp. 629–641, 2021.

[5] M. Saravana Kumar, S. R. Begum, and M. Vasumathi, "Influence of stir casting parameters on particle distribution in metal matrix composites using stir casting process," *Materials Research Express*, vol. 6, no. 10, Article ID 1065d4, 2019.

[6] V. Mohanavel, S. S Kumar, V. Sivaraman, V. K. Girish, and M. Ravichandran, "Tungsten carbide particulate reinforced AA7050 aluminum alloy composites fabricated by liquid state processing," *AIP Conference Proceedings*, vol. 2283, no. 1, Article ID 020087, 2020.

[7] A. A. Adediran, A. A. Akinwande, O. A. Balogun, and B. J. Olorunfemi, "Optimization studies of stir casting parameters and mechanical properties of TiO2 reinforced Al 7075 composite using response surface methodology," *Scientific Reports*, vol. 11, no. 1, pp. 19860–19920, 2021.

[8] M. Tebaldini, C. Petrogalli, G. Donzella, and G. M. La Vecchia, "Estimation of fatigue limit of a A356-T6 automotive wheel in presence of defects," *Procedia Structural Integrity*, vol. 7, pp. 521–529, 2017.

[9] H.-Y. Yang, Z. Wang, L.-Y. Chen, S.-L. Shu, F. Qiu, and L.-C. Zhang, "Interface formation and bonding control in high-volume-fraction (TiC+TiB2)/Al composites and their roles in enhancing properties," *Composites Part B: Engineering*, vol. 209, Article ID 108605, 2021.

[10] A. K. Srivastava, M. Maurya, A. Saxena, N. Kumar, and S. P. Dwivedi, "Statistical optimization by response surface methodology of process parameters during the CNC turning operation of hybrid metal matrix composite," *EVERGREEN Joint Journal of Novel Carbon Resource Sciences & Green Asia Strategy*, vol. 8, no. 1, pp. 51–62, 2021.

[11] A. M. Tiṭu, A V Sandu, A B Pop et al., "Design of experiment in the milling process of aluminum alloys in the aerospace industry," *Applied Sciences*, vol. 10, no. 19, p. 6951, 2020.

[12] S. J. S. Chelladurai, R. Arthanari, R. Selvarajan, R. Kanagaraj, and P. Angappan, "Investigation on microstructure and tensile behaviour of stir cast LM13 aluminium alloy reinforced with copper coated short steel fibers using response surface methodology," *Transactions of the Indian Institute of Metals*, vol. 71, no. 9, pp. 2221–2230, 2018.

[13] K. Mermerdaş, Z. Algın, S. M. Oleiwi, and D. E. Nassani, "Optimization of lightweight GGBFS and FA geopolymer mortars by response surface method," *Construction and Building Materials*, vol. 139, pp. 159–171, 2017.

[14] R. U. Owolabi, M. A. Usman, and A. J. Kehinde, "Modelling and optimization of process variables for the solution polymerization of styrene using response surface methodology," *Journal of King Saud University - Engineering Sciences*, vol. 30, no. 1, pp. 22–30, 2018.

[15] G. F. Aynalem, "Processing methods and mechanical properties of aluminium matrix composites," *Advances in Materials Science and Engineering*, vol. 2020, Article ID 3765791, 19 pages, 2020.

[16] M. Aziminezhad, M. Mahdikhani, and M. M. Memarpour, "RSM-based modeling and optimization of self-consolidating mortar to predict acceptable ranges of rheological properties," *Construction and Building Materials*, vol. 189, pp. 1200–1213, 2018.

[17] S. Zhao, H. Zhang, Z. Cui, D. Chen, and Z. Chen, "Particle dispersion and grain refinement of in-situ TiB2 particle reinforced 7075 Al composite processed by elliptical cross-section torsion extrusion," *Journal of Alloys and Compounds*, vol. 834, Article ID 155136, 2020.

[18] B.-X. Dong, Q Li, Z-F Wang et al., "Enhancing strength-ductility synergy and mechanisms of Al-based composites by size-tunable in-situ TiB2 particles with specific spatial distribution," *Composites Part B: Engineering*, vol. 217, Article ID 108912, 2021.

[19] Y. Ma, A Addad, G Ji et al., "Atomic-scale investigation of the interface precipitation in a TiB2 nanoparticles reinforced Al-Zn-Mg-Cu matrix composite," *Acta Materialia*, vol. 185, pp. 287–299, 2020.

[20] S. A. Kumar, A. Prabhu Kumar, B. Balu Naik, and B. Ravi, "Production and investigation on mechanical properties of TiC reinforced Al7075 MMC," *Materials Today Proceedings*, vol. 5, no. 9, pp. 17924–17929, 2018.

[21] A. Rai, B. Mohanty, and R. Bhargava, "Supercritical extraction of sunflower oil: a central composite design for extraction variables," *Food Chemistry*, vol. 192, pp. 647–659, 2016.

[22] G. Cibilakshmi and J. Jegan, "A DOE approach to optimize the strength properties of concrete incorporated with different ratios of PVA fibre and nano-Fe2O3," *Advanced Composites Letters*, vol. 29, Article ID 2633366X2091388, 2020.

[23] E. Alih and H. C. Ong, "An outlier-resistant test for heteroscedasticity in linear models," *Journal of Applied Statistics*, vol. 42, no. 8, pp. 1617–1634, 2015.

[24] C. Rajaravi, B. Gobalakrishnan, and P. R. Lakshminarayanan, "Effect of pouring temperature on cast Al/SiCp and Al/TiB2 metal matrix composites," *Journal of the Mechanical Behavior of Materials*, vol. 28, no. 1, pp. 162–168, 2019.

[25] V. R. Mehta and M. P. Sutaria, "Investigation on the effect of stirring process parameters on the dispersion of SiC particles inside melting crucible," *Metals and Materials International*, vol. 27, no. 8, pp. 2989–3002, 2021.

[26] K. R. Ramkumar, H. Bekele, and S. Sivasankaran, "Experimental investigation on mechanical and turning behavior of al 7075/x% wt. TiB2-1% Gr in situ hybrid composite," *Advances in Materials Science and Engineering*, vol. 2015, Article ID 727141, 14 pages, 2015.

[27] M. Ramesh, D Jafrey, and M. Ravichandran, "Investigation on mechanical properties and wear behaviour of titanium diboride reinforced composites," *FME Transactions*, vol. 47, no. 4, pp. 873–879, 2019.

[28] N. M. Rahma, K. M. Eweed, and A. A. Mohammed, "Investigation and improvement the properties of 7075 AL/T6 alloy using TiO2 nanomaterials," *IOP Conference Series: Materials Science and Engineering*, vol. 454, no. 1, Article ID 012144, 2018.

[29] G. B. V. Kumar, P. S. S. Gouda, R. Pramod, and C. S. P. Rao, "Synthesis and characterization of TiO2 reinforced Al6061 composites," *Advanced Composites Letters*, vol. 26, no. 1, Article ID 096369351702600, 2017.

[30] A. A. Adediran, K. K. Alaneme, I. O. Oladele, and E. T. Akinlabi, "Microstructural characteristics and mechanical behaviour of aluminium matrix composites reinforced with Si-based refractory compounds derived from rice husk," *Cogent Engineering*, vol. 8, no. 1, Article ID 1897928, 2021.